A SIMPLE MODEL OF ABOVE THRESHOLD IONIZATION

by

Argyrios Alexander Chatzipetros

Thesis submitted to the Faculty of the

Virginia Polytechnic Institute and State University

in partial fulfillment of the requirements for the degree of

MASTER OF SCIENCE

in

Electrical Engineering

APPROVED:

I. M. Besieris, Chairman

G. S. Brown

D. A. de Wolf

April, 1990

Blacksburg, Virginia

A SIMPLE MODEL OF ABOVE THRESHOLD IONIZATION

by

Argyrios Alexander Chatzipetros

I. M. Besieris, Chairman

Electrical Engineering

(ABSTRACT)

A simple model for above threshold ionization is presented in this work. It is based on modeling the pulsed laser beam involved in ionization as a *cylinder* consisting of elementary cells whose volumes are very small compared to the pulse volume. A cell is occupied by a number of photons determined probabilistically and found to follow the Poisson distribution. During ionization, resulting from the application of the laser field, a typical atom finds itself in one of the cells and one of its electrons absorbs the photon energy. The electron will be detached from its atom and will exit the interaction volume (the laser beam) if the energy contained in the particular cell is high enough. The model predicts all possible energies of the electrons exiting the beam and produces energy spectra associated with these electrons. While most of the other available models make only qualitative comparisons, we are able to make both qualitative and quantitative comparisons with experimental data.

Acknowledgements

I wish to express my gratitude to Professor I. M. Besieris for his advice, aid and guidance.

I am greatly indebted to Dr. A. M. Shaarawi and Dr. R. W. Ziolkowski for their technical guidance and their valuable contributions concerning various aspects of this thesis.

I wish to thank Professors G. S. Brown and D. A. de Wolf for serving on my M.S. advisory committee.

I am deeply appreciative of my family's support; especially that of my father Alexander, my mother Spyridoula, my brother Panagiotis, and my sister Gethsimani.

I would like to acknowledge my thanks to Mr. Apostolos Tsoukkas for the interesting discussions about the work presented here and for helping me in preparing the figures included in this thesis.

This work has been supported, in part, by Lawrence Livermore National Laboratory under contract No. 20812103.

Table of Contents

CHAPTER 1

INTRODUCTION

A very important phenomenon dealing with ionization is the photoelectric effect, whereby a light ray incident on a metal surface causes the detachment of electrons located on the surface from their parent atoms. The electrons, after obtaining enough energy, leave the surface with a certain velocity. Although it seems quite reasonable that increasing the light intensity will cause the release of more electrons, this is not always the case since the wavelength of the radiation is a crucial factor. The photoelectric effect is characterized by a critical wavelength above which no electrons are freed regardless of the light intensity. This feature cannot be accounted for by the classical framework describing the release of an electron by an external electromagnetic field.

To interpret these results, Einstein, in 1905, suggested a very simple explanation by introducing the concept of the photon. According to this idea, light consists of discrete quantities of energy called quanta or photons. The energy of a photon equals $\hbar\omega$, where $\hbar$ is Planck's constant divided by 2π, and ω is the frequency of radiation in rad/sec. Concerning the photoelectric effect, an electron that originally is in the ground energy state absorbs an energy equal to the photon energy and attains a kinetic energy which is only a fraction of the photon energy. The rest of the

energy is used by the electron to overcome the ionization potential that holds it attached to its parent atom. This process results in the advancement of the electron to a continuum (non discrete) energy state outside the metal.

One may wonder whether it is possible for an electron to actually absorb more than one photon. To answer this experimentaly, one could try to shine a ray of light of very high intensity on a metal and observe the electrons. Another possibility would be to choose an element whose ionization potential is large compared to that of a metal, so that release of electrons would result from absorption of more than one photon. The latter proved to be the correct approach and in 1965 Voronov and Delone [1] observed what is now called multiphoton ionization (abbreviated as MPI). The material utilized was xenon (Xe) and the electromagnetic radiation was a ruby laser. The ionization potential for Xe is 12.13 eV, while the photon energy for the ruby laser is 1.78 eV. Thus, ionization in this case results from the absorption of seven photons. The kinetic energy of the electron freed was, as before, smaller than the photon energy. Perturbation theory can explain all aspects of MPI. The electromagnetic field is much smaller than the Coulomb field that keeps the electrons attached to the nucleus. Perturbation theory then can be applied with the Coulomb field being the perturbed field while the electromagnetic field is the perturbation. The electron energy spectrum produced during an MPI experiment is graphically seen as the plot of energy versus the number N of photons absorbed, and consists of only one peak located at N_a, where N_a is the number of photons absorbed during ionization.

In recent years, more powerful laser sources became available. When these high-intensity laser beams were applied to the ionization problem, a new unexpected phenomenon occurred; specifically, the kinetic energy of a released electron was found to be larger than the photon energy! This phenomenon has been given the name "above threshold ionization" (abbreviated as ATI). Perturbation theory breaks down in this case, and cannot explain the mechanism. Here, the electromagnetic field (e.g., in a laser beam) is of the order of the Coulomb field and perturbation theory can no longer be applied. ATI was first observed in the six-photon ionization of xenon (Xe) at 10^{11} W cm^{-2} (a relatively low intensity) and with a photon energy of 2.32 eV [2]. In ATI, the

atom actually absorbs more photons than necessary (for ionization), and the energy of the free electron is larger than the photon energy.

In the beginning, it seemed that ATI could be explained by the lowest-order perturbation theory (abbreviated as LOPT). This was true until a new experiment by Kruit *et al.* in 1983 [3] produced energy spectra very different from the usual MPI spectra. The experiment dealt with the 11-photon ionization of Xe at a laser wavelength of 1064 nm and intensities close to 10^{13} W cm^{-2}. The energy spectrum of the electrons produced did not correspond to a single peak as expected from a LOPT analysis of N – photon ionization (N being the minimum number of photons needed for ionization). Instead, it consisted of a series of peaks evenly spaced by an amount equal to the photon energy. These peaks emerged as a result of absorption of additional photons. In addition to this, the first peak of the spectrum was missing and the amplitude of the other peaks did not decrease as normally expected, and the intensity dependence of the amplitudes did not follow the I^{N+S} power law as expected by the lowest order perturbation theory (S being the extra number of photons absorbed). The different structure of the spectra first observed by Kruit *et al.* was verified once more by an experiment conducted by Lompre′ *et al.* in 1985 [4] on the ionization of neon (Ne) and helium (He) at 1064 nm wavelength and high laser intensities (of the order of 10^{14} W cm^{-2}). One important difference between the two experiments mentioned above was that the electrons released during the latter experiment had much higher kinetic energies. Specifically, in the ionization of Ne at an intensity of about 8×10^{14} W cm^{-2} and at 1064 nm, electrons with energies greater than 60 eV were detected corresponding to the absorption of about 52 photons! In the case of He, 68 photons were absorbed at 1064 nm and 1×10^{15} W cm^{-2}. Another equally important difference between the two experiments was the fact that more than one low energy peak was missing at the low energy part of the spectra in the Lompre′ experiment. For instance, on ionization of He, with the laser wavelength and intensity specified above, the first 26 peaks were completely absent from the spectrum. Later, in an experiment by Luk *et al.* [5], a smaller wavelength was used (248 nm), and even though the intensity was high enough (of the order of 10^{14} W cm^{-2}), almost no peak suppression was observed. Another interesting ATI experiment was the one conducted by Bucksbaum *et al.* [6] in 1986. The energy spectra produced there revealed

that peak suppression was more prominent when the external electromagnetic field was circularly polarized as compared to suppression due to a linearly polarized field. Thus, it became clear that high intensity, long wavelength and circular polarization were three important ingredients for peak suppression.

With the availability of new experimental data, numerous scientists have become interested in ATI and have suggested several approaches to interpret it. The most successful theories to date are based on an old idea of Keldysh [7]. As a final state they use the one for a free electron in an electromagnetic field; it is called the "Volkov state". There are two electric field strengths involved in ionization. One of them is the Coulomb field which always exists in an atom-electron system and is responsible for holding an electron close to its parent atom. The other one is the external electromagnetic field. At relatively low intensities, the Coulomb field is much stronger than the external field, whereas at high intensities the roles switch. So at high intensities the Coulomb field, being much weaker than the electromagnetic field, is neglected. In treating ATI, one then uses the Volkov state which is an exact solution for the system of one electron interacting with a plane electromagnetic field. Using this solution results in the typical ATI-spectra structure. Since this approach does not include the Coulomb field, it is obvious that it is not appropriate in the limit of low intensity and, as Pan [8] says, "many features of multiphoton ionization, such as angular distribution and resonant structure, cannot be correctly described with this approach."

An attempt to modify the Volkov state approach to include the effects of the Coulomb potential was made by Pan [8]. His wavefunction is a Coulomb wave modified by infinite-order field coupling, and it is also a modified Volkov state in the sense of replacing plane waves by Coulomb waves. Even though this theory seems to be more complete than the others, difficulties in obtaining better analytical expressions for the equations derived do not allow satisfactory qualitative as well as quantitative comparisons with experimental results.

Most theoretical methods on ATI refer to one-electron calculations. Experiments on ATI involve many-electron atoms most of the time. One then wonders whether these theoretical "mono-electron" models could be able to thoroughly explain all features of ATI, especially multiple ionization that has been observed in some experiments [9,10,11]. A few attempts have been made

to develop multi-electron theoretical models that include multiple in addition to single electron ionization. Such a model is the one by Trombetta *et al.* [12]; it has been applied to the ionization of He, however with little success due to the numerous approximations made.

Most of these theories lead to relatively good qualitative agreements with the energy spectra produced in experiments. It is generally accepted, for example, that the ATI spectrum for high intensities is bell-shaped [12]. Quantitative agreements with the experimental spectra, on the other hand, are rare due to mathematical difficulties in obtaining simple analytical expressions and due to numerous approximations made as mentioned above. It is obvious that a complete theory that will be able to explain all aspects of ATI is needed.

Our approach to ATI is based on a novel modeling of the laser beam involved in ionization. It consists of a representation of photons as bump-like fields or pulses which are exact solutions of the scalar wave equation and can accommodate simultaneously the corpuscular and wave aspects of light. An expression for the photon "radius" can be ascertained and it is directly proportional to the radiation wavelength. The photon is assumed to be a sphere whose volume is given in terms of this radius. Next, a crude model for a laser pulse is given as a *cylinder* containing elementary spheres (photons). The volume of the laser pulse is directly proportional to the pulse duration and to the square of the radius of focus of the laser beam. The energy of the pulse is directly proportional to the volume and the intensity of the pulse. As we mentioned above, the laser pulse is seen as an aggregate of spherical cells each having a volume equal to the photon volume. The number of cells in the pulse is just the pulse volume divided by the cell volume and the number of photons in the pulse is the pulse energy divided by the photon energy. The probability that a cell contains a specific number of photons is found and results in the Poisson formula. During ionization, a typical atom finds itself in the interaction volume (pulse volume). The size of the atom is of the order of the photon size and the probability that two atoms occupy the same cell is negligible. In a laser beam, a typical cell will contain a specific number of photons, and an atom located in that cell will absorb this number of photons. Therefore, by applying the Poisson formula, we can produce electron energy spectra and compare them with the experimental ones. In addition to good

qualitative agreements, our ATI model exhibits good quantitative agreements with experimental data.

In Chapter 2, we shall describe some of the existing theoretical attempts to explain ATI. In particular, we shall discuss in detail a theoretical approach based on considering the final states as Volkov states. Also in Chapter 2, we shall give a description of typical ATI experiments and the difficulties associated with them. In Chapter 3 we shall describe the characteristics of the special pulses mentioned above. A photon model, based on these pulse properties, will be presented. In Chapter 4, our theoretical ATI model will be given and comparisons to experimental data will be shown. Difficulties associated with ATI experiments will be mentioned. Limitations and advantages of our ATI model, as well as future considerations, will also be discussed.

CHAPTER 2

EXISTING THEORY OF ATI AND EXPERIMENT

2.0 INTRODUCTION

In this chapter we shall first provide a historical background on the photoelectric effect, the multiphoton ionization, and finally on ATI. Then we shall give a general picture of the theoretical work on ATI which involves a general description of a few methods. These methods consist of developing models that treat effects on an electron bound by a short-range potential. One of them is the work done by Reiss [13,14], which describes the effect of an intense electromagnetic field on a weakly bound system. It is based on a relatively old idea introduced by Keldysh. It is essentially an approximation method according to which the binding potential is neglected when considering the final state of the detached electron. The effect that dominates in the final state regime is that due to the intense electromagnetic field. The essential difference between this formalism and the one expounded by Keldysh is in the choice of a gauge. Reiss chooses a radiation gauge in which the external electromagnetic field is expressed. This makes the method simpler and more tractable

[13]. The formalism is applied to finding transition probabilities for any order of interaction with both linearly and circularly polarized plane wave fields. With the assumption that the field leaves the neutral atomic core relatively unaffected, the formalism is applied to the example of a negative hydrogen ion irradiated by circularly or linearly polarized 10.6 μm radiation. Most of the theoretical work used to explain ATI is based on this idea, and so far it has proven to be, to our knowledge, the most successful one.

In this chapter we shall also discuss existing ATI experiments as well as the difficulties associated with them, such as the determination of the laser intensity and the problem of space charge.

2.1 HISTORICAL BACKGROUND

Einstein, in 1905, suggested an extremely simple explanation of the photoelectric effect. It was based on the idea that light consists of discrete quantities of energy called photons. A typical matter interacting with light will only absorb an integer number of photons. According to Einstein, a typical freed electron has a kinetic energy which is a fraction of the photon energy and it is given by

$$\frac{mv^2}{2} = E_e = \hbar\omega - W, \tag{2.1.1}$$

where W is the work necessary to get the electron out of the atom and $\hbar\omega$ is the photon energy. Eq. (2.1.1) is Einstein's law; it can be rewritten in the form

$$E_e = \hbar\omega - E_i, \tag{2.1.2}$$

where E_i is the ionization potential of a single atom. A typical electron that originally is in the ground energy state $|g>$ obtains enough energy from the electromagnetic radiation and advances to a continuum (non discrete) state $|c>$, as seen in Fig. 2.1. The probability w for this transition

can be calculated through time-dependent perturbation theory and, using the Fermi Golden Rule [15], is found to be

$$w = (2e^2/n)I| < c|z|g > |^2 , \tag{2.1.3}$$

where z denotes position, e is the electron charge, n is a normalization constant and I is the intensity of the electromagnetic field E; the latter is related to E by

$$I = (\varepsilon_0 c/2)E^2 , \tag{2.1.4}$$

where ε_0 is the vacuum permittivity and c is the speed of light.

Absorption of more than one photon is called multiphoton absorption, during which matter can be ionized by simultaneous absorbtion of several photons provided the intensity is high enough. The transition probability in this case, obtained through perturbation theory and by applying the Golden Rule, is proportional to the Nth power of the intensity I [16]. This is the so called I^N power law. During multiphoton ionization (abbreviated as MPI) and at moderate laser intensities, the electron absorbs N photons and is released with a kinetic energy

$$E_N = N\hbar\omega - E_i \tag{2.1.5}$$

which is smaller than the photon energy $\hbar\omega$.

When high-intensity laser beams are used, new ionization phenomena occur; specifically, the kinetic energy of a released electron can be larger than the photon energy. This phenomenon has been given the name "above threshold ionization" (abbreviated as ATI). The atom, in this case, actually absorbs more photons than necessary (for ionization). The energy of the released electron is given by

$$E_e = (N + S)\hbar\omega - E_i , \tag{2.1.6}$$

where N is the number of photons necessary for ionization and S the number of extra photons absorbed.

Numerous experiments on ATI have been performed. The results have indicated that ordinary perturbation theory is inadequate to explain ATI. The energy spectrum of the electrons produced in the experiments consists of a series of peaks that are evenly spaced, by an amount equal to the photon energy, and have different amplitudes. At relatively low intensities, the peaks decrease from left to right. However, as the intensity increases, the peaks corresponding to lower-energy electrons (left of spectrum) decrease and eventually disappear as seen in Fig. 2.2. The peak spacing is still equal to $\hbar\omega$.

2.2 THEORETICAL METHODS

Most of the theoretical work used to explain ATI is based on considering the electron final states as Volkov states [13,17,18]. The different electric field strengths involved in ATI vary as the laser light intensity varies. A laser intensity of 10^{13} W cm^{-2} corresponds to a peak electric field of 10^{8} V cm^{-1} . The Coulomb field in the initial state is about 10^{9} V cm^{-1}, well above the laser field. In the 'free' state reached by the ionization process, it is 10^{7} V cm^{-1}, which is ten times smaller than the laser field, and thus can be neglected. It is then that the electron is freed.

One particular theoretical model, based on the idea discussed above, is the one developed by Reiss [13]. It is applicable to the photodetachment by a plane wave field of an electron bound by a short-range potential. The technique involved is a revision and extension of an approximation method introduced by Keldysh, whereby the binding potential is neglected in comparison to the external electromagnetic field effects on the final state of the freed electron during ionization. The electron final state is considered as a Volkov state; that is, a state where an electron is released into a strong electromagnetic field (e.g., a laser field) and not in vacuum. Through this method, transition probabilities can be found for any order of interaction for both linearly and circularly polarized plane-wave fields. Later in this section, we shall discuss this formalism in connection with a negative hydrogen ion irradiated by 10.6 μm radiation. The resulting transition probability will be used to compare the predicted spectra with the ones obtained for the case of xenon ionization in two

experiments chosen by Reiss. The Reiss' model is based on neglecting the effect of the binding potential by comparison to the field effects on the final state of the detached electron. The essential difference between the work of Reiss and Keldysh lies in the choice of gauge in which the external electromagnetic field is expressed. Keldysh uses the electric field gauge, whereby the interaction Hamiltonian is given by $\vec{H} = -e\vec{F} \cdot \vec{r}$, $\vec{F}$ being the electric field vector; Reiss, on the other hand, uses the radiation gauge, with $\vec{H} = -m^{-1}e\vec{A} \cdot (-i\vec{\nabla}) + (2m)^{-1}e^2|\vec{A}|^2$, where $\vec{A}$ is the vector potential of the applied field and the convention $\hbar = c = 1$ is used. This gauge choice makes the formalism much simpler and more tractable.

The transition probabilities are calculated through the $S-$matrix. The applied electromagnetic field is treated in the radiation gauge and the wavefunctions used are the long-wavelength approximation Volkov solutions. In principle, the field can be any wave packet which vanishes at infinite times, subject to the limitations that the frequency components of the packet must all propagate in the same direction and must satisfy the long-wavelength approximation. In writing the $S-$matrix a monochromatic plane wave is assumed. Moreover, the long-wavelength approximation is used in expressing the vector potential.

The final form of the differential total transition probability per unit time $dW/d\Omega$ arising from monochromatic circularly polarized electromagnetic fields is a closed-form analytical expression provided there is an analytical form for the initial state wavefunction in the momentum representation. It involves the sum over n of $J_n^2(z^{1/2}\gamma)$, where J_n is the nth order ordinary Bessel function, z is the intensity parameter defined below, and $\gamma = (2/m\omega)^{1/2}p\sin\theta$, where θ is the angle of emmission of the electron measured with respect to the direction of the field propagation. In the expression for γ the quantity p is defined as

$$p = (2m\omega)^{1/2}(n - z - \varepsilon_B)^{1/2}\,, \tag{2.2.1}$$

where $\varepsilon_B \equiv E_B/\omega$, with E_B being the binding energy and $z = e^2E^2/4m\omega^3$, with E being the amplitude of the electric field vector. Equation (2.2.1) is a conservation condition. The underlying physics is most easily seen in the quadratic form

$$p^2/2m = (n - z - \varepsilon_B)\omega \,. \tag{2.2.2}$$

Consider first this expression in the low-intensity limit $z \to 0$. In this case, Eq. (2.2.2) says that the final kinetic energy of the freed electron is given by the energy contributed by the nth-order interaction with the field (the energy of n photons, $n\omega$), minus the energy needed to overcome the initial binding energy E_B of the electron. For $z \neq 0$, the energy $z\omega$ is a minimal interaction energy of the electron with the electromagnetic field.

Equation (2.2.2) implies that n is bounded from below, i.e., $n \geq z + \varepsilon_B$. Since n is an integer, one can write

$$\begin{aligned} n &\geq n_0 \,, \\ n_0 &= [z + \varepsilon_B] \,, \end{aligned} \tag{2.2.3}$$

where $[x]$ is the largest integer not exceeding x. Since n is the number of photons participating in ionization, Eq. (2.2.3) shows that a sufficient increase in intensity will cause the lowest-order peaks to disappear.

As in the circular polarization case, $dW/d\Omega$ for linear polarization is an entirely analytic expression as long as an analytic form for the momentum-space initial wavefunction exists. However, in the linear polarization case, dW/Ω has a more complicated structure than the one corresponding to the circular polarization case.

There are some limitations in this analysis. First, there is the assumption associated with equation (2.2.3). The binding potential V_B is not affected by the introduction of the applied field potential V_A and, being of finite range, its effect can be neglected when comparing it to the field effect on the final state of the detached electron. In numerous physical problems the above assumption is not valid. Consider for example the photodetachment of a negative hydrogen ion, where V_B is the binding potential of an electron to a neutral hydrogen atom. The atom is itself polarized under the application of the external field and this causes V_B to change. Another limitation is the fact that the procedure in obtaining the $S-$matrix does not take into account the possibility of intermediate resonances associated with the binding potential. During ionization of a

neutral atom, there is a possibility that a number of photons, smaller than the number needed for ionization, will be resonant with an excited bound state. Ionization, then occurs in two stages: excitation, followed by ionization from the excited state. Finally, there is a constraint relating to depletion effects, which can take place when the total transition probability W is of the order of $(\Delta t)^{-1}$, where Δt is the duration of the electromagnetic pulse.

The negative hydrogen ion H^- was selected by Reiss as an example with which to apply his formalism. It is assumed that H^- has only one bound state. The binding potential is of finite range, in view of the neutrality of the residual atom after ionization. The differential transition probability per unit time for a circularly polarized applied field was obtained by Reiss in 1987 [14] and two comparisons were made of his formalism with experimental data for the circular polarization case. The first comparison, shown in Fig. 2.3, dealt with the spectrum obtained in 1986 by Yergeau *et al.* [19] for the photoionization of Xe by circularly polarized light of 1064 nm and at an intensity of 4×10^{14} W cm^{-2}. In that case the theory produced a spectrum with unrealistically small probabilities at the low energy end of the spectrum. In the second comparison, shown in Fig. 2.4, the experimental data obtained by Bucksbaum *et al.* in 1986 [6] were used. The intensity in this experiment was stated to be 1.5×10^{13} W cm^{-2}. However, Reiss made the comparison pressuming that the intensity was about 1.53 times larger since that could be possible. The agreement in that case was much better than with the former comparison.

2.3 ATI EXPERIMENTS AND DIFFICULTIES

2.3.1 Experimental Set-ups

A basic experimental picture is given in Fig. 2.5. Box (1) represents the laser. Part of the laser beam is reflected on mirror (2) and onto lens (3). Then it is focused on region (4); a region where atoms are located in a vacuum chamber of very low pressure. Ions are formed in that focused re-

gion where an electric field (5) is applied to draw them out to the collector (6). Part of the laser radiation is transmitted through mirror (2) and, after being attenuated by neutral filters (7), is incident on lens (8) which is identical to lens (3) and located at the same distance from the laser. The spatial distribution of the illumination in the focused region is photographed on an enlarged scale by means of micro-lens (9) and photographic film (10). The vacuum chamber can be pumped down to very low pressures (of the order of 10^{-7} Torr) into which a rare gas is leaked (up to a total pressure of nearly 10^{-5} Torr [20]). The pressure is very low; this makes the number of atoms inside the vacuum chamber small so that no atom collisions occur. The laser beam involved in the experiment is focused in this atomic medium and the ions are collected and mass analysed by a time-of-flight (TOF) mass spectrometer.

The lasers used in ATI experiments are commercial picosecond Nd: YAG lasers. The laser pulse can be amplified up to 3 GW at 1064 nm. The second harmonic can be generated at 532 nm up to 1.5 GW when needed [20]. Energies up to 100 mJ per laser pulse are available at 1064 nm and of about 30 mJ at 532 nm, which after focusing down to a diameter of about 30 μm, yields an intensity of more than 10^{14} W cm^{-2} which is more than necessary to study the 11-photon ionization of xenon [21]. The bandwidth-limited pulse is 30 psec in duration. It can be varied when required from 30 to 200 psec. The laser pulse is focused into the vacuum chamber by a 150 mm focal length lens. The focused intensity distribution is determined from photometric measurements. The laser intensity is adjusted to produce between 1 to 10^4 electron-ion pairs in the interaction volume [20].

Energy analysis of the electrons produced in the ionization volume is performed using a retarding-potential system when the electron energy spectrum consists of a very large number of peaks and a magnetic-field paralleliser electron time-of-flight spectrometer when the electron energy spectrum consits of a few peaks [20].

2.3.2 Experimental Difficulties

The first difficulty has to do with the laser intensity. In experiments such as the one discussed in the previous subsection the intensity is generally above 10^{14} W cm^{-2}. "High intensities of this kind are currently achieved in tightly focused picosecond laser pulses and also in the spikes of multimode nanosecond laser pulses." [21]. It is extremely difficult to measure the instantaneous intensity when using nanosecond pulses, and in the case of picosecond pulses the intensity is not usually trusted to better than a factor of 2. This difficulty can be partially dealt with by assuming that the saturation intensity for an MPI process (the peak laser intensity at which, for a given pulse duration, the ionization probability equals 1), is known. Under this assumption, the intensity used in a typical experiment can be referenced to the saturation intensity of the ATI process under study, permitting a comparison among different experiments after correction of the pulse-length differences (when they can be measured) [21].

A second serious difficulty encountered in these experiments is that of space charge. During an ATI process electrons are produced having high or low energies, depending on the number of photons they absorb. The high energy electrons leave the interaction volume much faster than the low energy ones, leaving behind a net positive charge that can slow down the other electrons, or even immobilize them. This obviously leads to changes in the electron energy spectra. These changes are of the same nature as the high-intensity effects observed in ATI experiments (suppression of low-energy electron peaks), and therefore the experimentalist should be very careful to avoid them, keeping in mind that the magnitude of the effect depends on the spreading of the spectrum. The best way to get rid of space charge is to work with as few ionization events as possible in the interaction volume and to use a highly efficient method for collecting electrons. One then has to face the problem of obtaining small ionization signals at high intensities. This can be done by decreasing the atomic density as much as possible, taking into account the ionization of the background gases, and/or decreasing the interaction volume [21].

2.4 CONCLUSION

A description of a few theoretical models dealing with ATI is given in this chapter, with particular emphasis on a method developed by Reiss, which is applicable to the photodetachment by a plane-wave field of an electron. It is an approximation technique very closely related to that of Keldysh, which is based on the neglect of the binding effects as compared to the strong external field. Reiss' method makes use of the Keldysh approximation for the $S-$matrix. The $S-$matrix is used in turn, for the calculation of a general differential transition probability per unit time, and the total transition probability per unit time for an electron released during ionization. Both circular and linear polarizations of the field can be accomodated. The expressions obtained for the probabilities are different for different polarizations, with a much more complicated expression for the linear polarization case. The transition probabilities are found to depend on a general intensity parameter $z = e^2a^2/4m\omega$, where a is the magnitude of the radiation-gauge vector potential of the applied field of circular frequency ω.

Limitations of Reiss' model are also discussed in this chapter. Those are, the neglect of the binding potential and the fact that no intermediate resonances are considered. Another important limitation has to do with depletion effects, which can occur when the total transition probability W is of the order of $1/\Delta t$, where Δt is the duration of the electromagnetic pulse. An application of Reiss' formalism to the example of the photodetachment of the excess electron from an H^- ion by a $10.6-\mu$m radiation is given. The resulting transition probability is used to compare the predicted spectra with the spectra obtained for the case of ionization of xenon for circular polarization. The first comparison leads to a gross disagreement between the two spectra on the left side. The second one is better, however, only under Reiss' assumption that the intensity involved in ionization is about 50% larger than the stated experimental value.

Also presented in this chapter is a description of typical ATI experiments, as well as information on the laser system and the energy analysis of the released electrons. Experimental diffi-

culties are also discussed, e.g., the exact determination of the laser intensity and the problem of space charge.

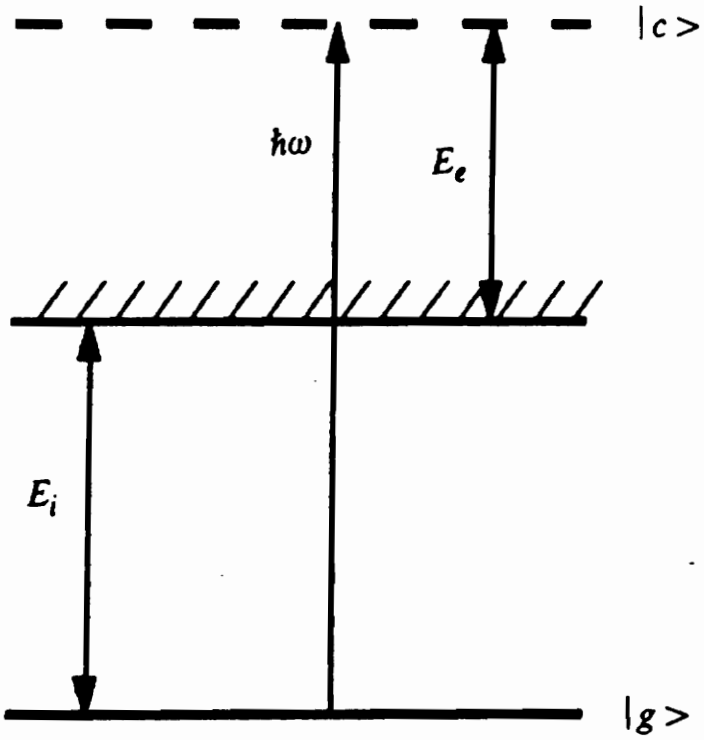

Fig. 2.1. Energy level diagram for the photoelectric effect.

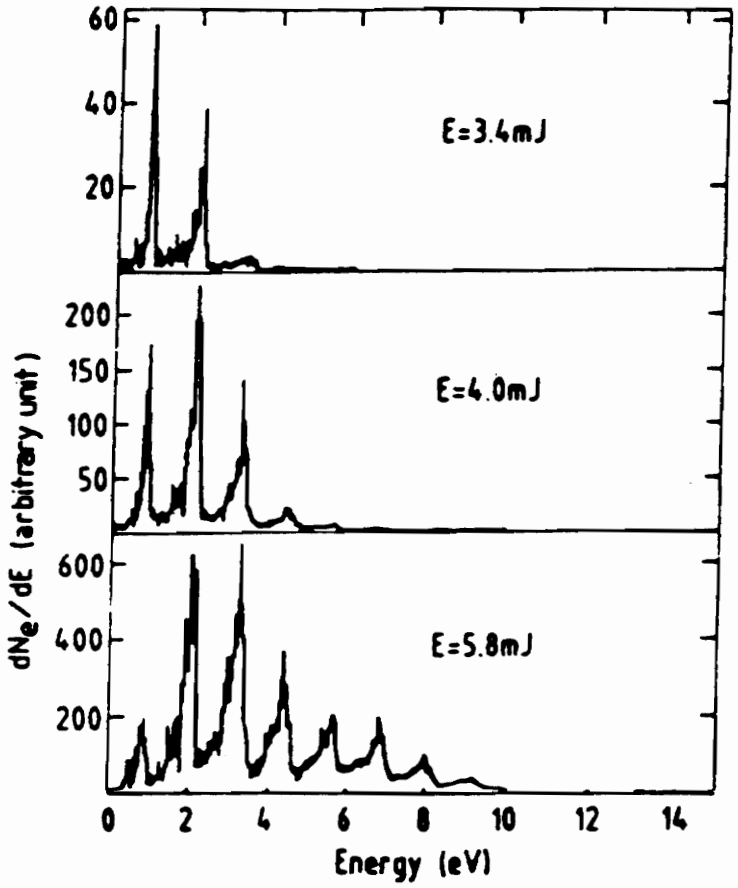

Fig. 2.2. Intensity dependence of the ATI electron energy spectrum [16].

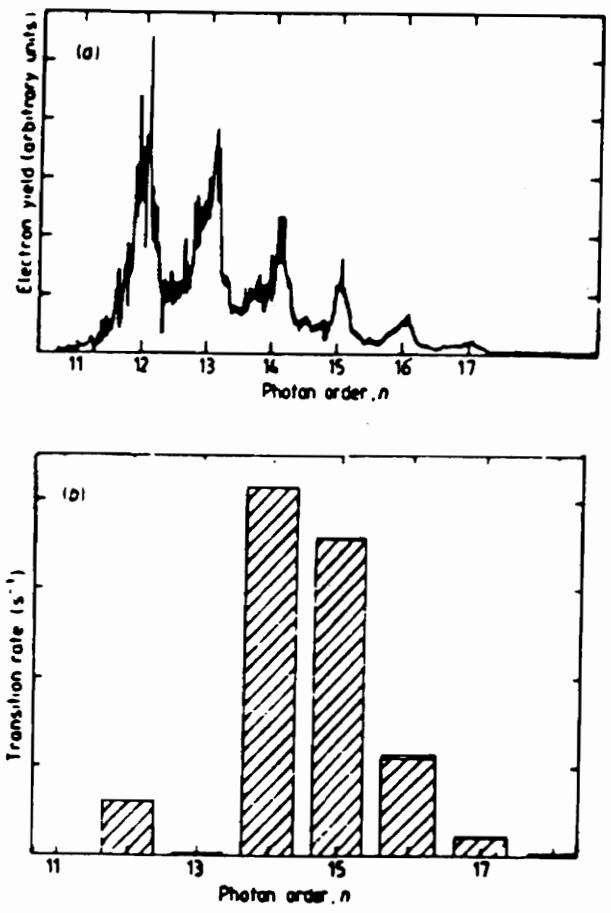

Fig. 2.3. Comparison of Reiss' theory to experimental ATI spectra. (a) Experimental electron spectrum of multiphoton ionization of xenon with circularly polarized light of 1064 nm. The intensity is about 4×10^{14} W cm^{-2}. (b) Theoretical spectrum corresponding approximately to the conditions of (a).

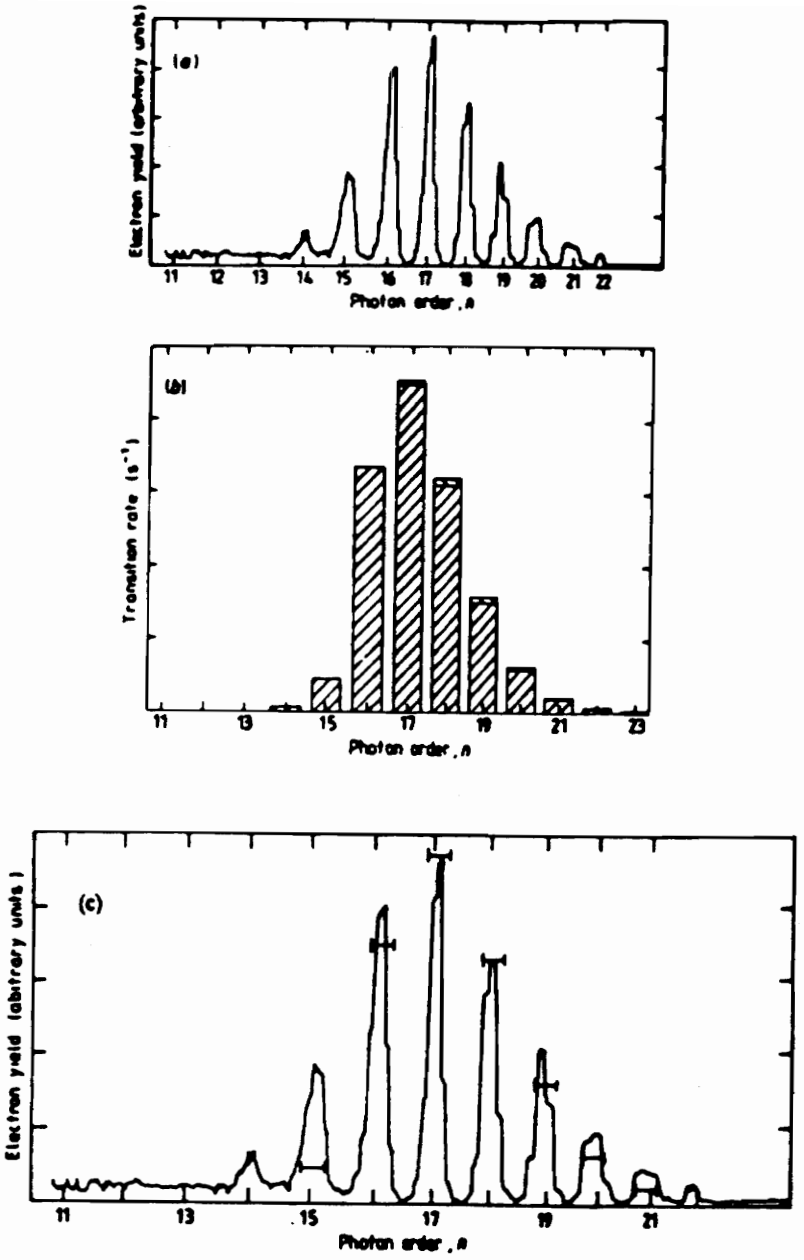

Fig. 2.4. Comparison of Reiss' theory to experimental ATI spectra. (a) Experimental electron spectrum of multiphoton ionization of xenon with circularly polarized light of 1064 nm. The intensity is about 1.5×10^{13} to 2.0×10^{13} W cm^{-2}. (b) Theoretical spectrum corresponding approximately to the conditions of (a). (c) Comparison of the experimental results (a) with the theoretical results of (b) represented by the horizontal bars superimposed on each of the peaks. The heights are scaled to match at $n = 18$.

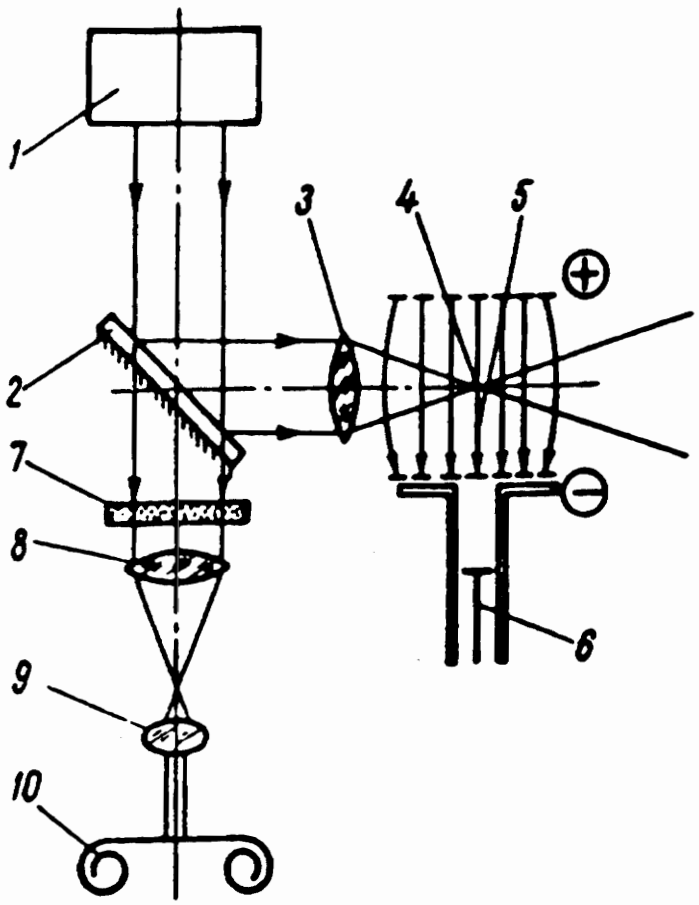

Fig. 2.5. Experimental set-up [1].

CHAPTER 3

FOCUS WAVE MODES AND THE PHOTON MODEL

3.0 INTRODUCTION

A nondispersive wave packet representation of photons is presented in this chapter. Such a wave packet belongs to a class of exact, continuous and nonsingular solutions to the scalar wave equation and Maxwell's equations, with centers that travel at the speed of light in straight lines. For such a wave packet, the energy density of the field around the center is extremely high compared to the rest of the field. The amplitude of the central bump of the field increases while its spatial extent decreases as the wavelength of the light is decreased. These properties allow the central bump to depict the corpuscular character of light. At the same time, the background field can account for the wave properties of light. The material presented here is derived from the work done by Shaarawi, Besieris and Ziolkowski [22].

3.1 THE FWM PULSE

It is our aim in this chapter to consider the possibility of modelling light by bump-like fields or pulses that can accomodate simultaneously the corpuscular and wave aspects. The synthesis of such solutions is achieved by recently developed novel approaches to the synthesis of wave signals [23-26].

An interesting solution to the scalar wave equation and Maxwell's equations that has been studied extensively recently is the Focus Wave Mode (FWM) [23-26]. Our purpose in this section is to emphasize some of its properties which make it very appealing for modelling photons. We shall consider only the scalar form of this pulse.

The three-dimensional, zeroth order, FWM pulse

$$\Psi(\vec{r}, t) = \frac{A(\beta)}{4\pi\,(a_1 + i(z - ct))}\; e^{-\beta\rho^2/(a_1 + i(z-ct))}\; e^{i\beta(z+ct)} \tag{3.1.1}$$

is an exact solution to the scalar wave equation [24]. Here, z is the direction of propagation, t is the time, c is the speed of light, ρ is the transverse radial variable, β is a characteristic wave number, a_1 is a parameter determining the width of the pulse and $A(\beta)$ is an amplitude factor. The FWM consists of a Gaussian envelope moving in the positive z-direction, modulated by a plane wave moving in the opposite direction. This solution does not disperse with time and it is nonsingular for all points of space time. At the center of the pulse ($z = ct$, $\rho = 0$), the waist of the envelope w is equal to $(a_1/\beta)^{1/2}$. For a_1 very small (i.e., for a pulse of a small waist), the solution given in Eq. (3.1.1) behaves like a localized Gaussian pulse moving in the positive z-direction, while for large a_1, such that $\beta a_1 \gg 1$, the solution looks more like a plane wave moving in the negative z-direction. Under the more stringent condition $\beta a_1 \ll 1$, the pulse has a large amplitude proportional to $1/a_1$ around its center, where $(z - ct) < a_1$ and $\rho < (a_1/\beta)^{1/2}$. Outside this portion of the pulse the amplitude falls off as $1/(z - ct)$ along the direction of propagation. At the same time the Gaussian

envelope stretches out in the transverse direction, with a waist $(z - ct)/(\beta a_1)^{1/2}$ that increases as we move away from the central part of the field.

The FWM, with the appropriate choice of $a_1 \ll 1$ m, looks like a localized "bump" field with a large amplitude around the center, incorporated in an extended nonlocal "background" field of a very low amplitude. This pulse is only localized around $z = ct$ within the waist w, while the rest of its field fans out to cover relatively larger distances in the transverse direction away from the center. It is this property that allows the field of the FWM to feel the two slits in Young's experiment, even though the central bump field is fairly localized [27]. For such a bump field one can associate the corpuscular aspects of light with its central portion of large amplitude. This localized bump is a part of an extended background wave structure of much lower field intensities. Thus, the wave and particle aspects of light can be brought together into a single framework. This interpretation agrees with de Broglie's conception of wave-particle duality, whereby the wave and the particle aspects of reality should exist simultaneously. It also reflects Einstein's concept of a particle as a highly concentrated "bunch" field that remains localized and does not disperse in free motion.

3.2 THE PHOTON MODEL

The waist of the central bump of the photon can be modelled as follows [22]:

$$w^2 = \left(\frac{\alpha}{8\pi}\right)^2 \left[\eta^2\lambda^2 + 3\lambda\lambda_c\right], \tag{3.2.1}$$

where α is the fine-structure constant, η a parameter of O(1), λ is the radiation wavelength and λ_c the Compton wavelength. The first term on the right side of Eq. (3.2.1) is related to atomic processes and the second one arises from particle interactions with photons.

It is interesting to note that the first term on the right side of Eq. (3.2.1) dominates at laser wavelengths of 1064 nm and 532 nm involved in ionization. At the wavelength λ_c, the energy of

the photon $\sim 0.01 m_e c^2$, which makes $\lambda_c = .24$ nm. So, $\lambda \gg \lambda_c$ in our case and the second term of the right hand side of Eq. (3.2.1) can be neglected. Eq. (3.2.1) then becomes

$$w^2 = \left(\frac{\alpha}{8\pi}\right)^2 \eta^2 \lambda^2 . \tag{3.2.2}$$

The photon radius r_γ is [22]

$$r_\gamma \equiv 2w = \eta \frac{\alpha\lambda}{4\pi} \tag{3.2.3}$$

Eq. (3.2.3) is the final form of the photon radius which will be used in treating ATI.

3.4 CONCLUSION

In this chapter, we have described a wave packet representation of light that can accommodate simultaneously its wave and its corpuscular character. The mental picture associated with the photon presented here is that of a localized bump that does not spread out as it travels in free space with the speed of light. The energy density of this bump is much larger than that of the tails. As seen in Eq. (3.2.3), the size of the photon is directly proportional to the wavelength. The cross-sectional area of the photon varies as λ^2 for atomic processes, or as $\lambda\lambda_c$ for interactions with individual particles, λ_c being the Compton wavelength of the particle involved in the interaction. At laser wavelengths of 1064 and 532 nm used in ATI experiments, $\lambda \gg \lambda_c$ leading to Eq. (3.2.3) which is the final photon radius model used in our ATI model considered in detail in the next chapter.

CHAPTER 4

THE FWM BASED ATI MODEL

4.0 INTRODUCTION

In Chapter 3 we demonstrated the feasibility of modeling photons by FWMs, i.e., bump-like fields or pulses that can accommodate the corpuscular and wave aspects of light simultaneously. Motivated by this photon representation, we will attempt to create a model for ATI. Before this is done, a model of the laser beam involved in ionization, will be introduced. The laser beam will be modeled as an aggregate of elementary spherical cells, each having a volume equal to the photon volume. It will be shown that the photon distribution in the beam follows a Poisson distribution. This laser beam model will be used to complete our ATI model. Comparisons with experimental data will be made and limitations and advantages of the ATI model as well as future considerations will be discussed.

4.1 LASER BEAM MODEL

The laser beam involved in above threshold ionization is extremely important. Knowledge of its exact characteristics is crucial in explaining several of the difficulties associated with ATI. A complete physical understanding of the beam is presently unavailable, and very high laser intensity values make the task even more difficult. One then is faced with the problem of obtaining a realistic laser beam model in order to examine the ATI phenomenon.

In Chapter 3, a wave packet representation of light was introduced. For such a wave packet, the energy density of the field around the center is extremely high compared to the rest of the field. The amplitude of the central bump of the field increases while its spatial extent decreases as the wavelength of the light increases. These properties allow the central bump to depict the corpuscular character of light. A photon model was postulated, according to which the waist of the photon is expressed as

$$w^2 = \left(\frac{\alpha}{8\pi}\right)^2 \left[\eta^2\lambda^2 + 3\lambda\lambda_c\right] . \tag{4.1.1}$$

where η is a free parameter of O(1), α is the fine-structure constant, λ is the laser wavelength, and λ_c is the Compton wavelength. The photon radius, r_γ, is given in terms of the photon waist as follows:

$$r_\gamma = 2w = \frac{\alpha}{4\pi}\left[\eta^2\lambda^2 + 3\lambda\lambda_c\right]^{1/2} . \tag{4.1.2}$$

The first term on the right hand side of Eq. (4.1.2) dominates at laser wavelengths of 1064 nm and 532 nm involved in ionization. At the wavelength λ_c, the energy of the photon is given approximately by $0.01 m_e c^2$ [22], which yields $\lambda_c = .24$ nm. As a concequence, $\lambda \gg \lambda_c$ and the second term on the right hand side of Eq. (4.1.2) can be neglected, resulting in the approximate relation

$$r_\gamma \simeq \eta \frac{\alpha\lambda}{4\pi} . \tag{4.1.3}$$

A wavelength of 532 nm corresponds to a photon radius of ($\eta \times 618$) pm. The atomic radii of helium, neon, and xenon are 180 pm, 160 pm, and 220 pm, respectively [28]. Since the parameter η is O(1), it is seen that the photon radius is of the order of the atomic radii of rare gases. Eq. (4.1.3) is the final form of the photon model which will be used in treating ATI.

We hypothesize next that each photon occupies a spherical volume of radius r_γ defined above. A crude model for a laser pulse consists in representing it as a *cylinder* consisting of these elementary spheres (photons). The volume of a pulse is then given by

$$V_p = \pi r_f^2 T_p c , \tag{4.1.4}$$

where V_p is the pulse volume in m^3, r_f is the radius of focus of the laser beam in meters, T_p is the pulse duration in seconds, and c is the speed of light in vacuum (3×10^8 m/sec). As seen in Eq. (4.1.4), the pulse volume is directly proportional to the pulse duration.

The energy E_p of the pulse is related to its intensity I by the relation

$$E_p = \pi I r_f^2 T_p , \tag{4.1.5}$$

where E_p is in Joules, r_f in centimeters, T_p in seconds, and I in W cm^{-2}. The units for r_f and I include centimeters here because I is expressed in W cm^{-2} in experiments. The intensity of the pulse is directly proportional to the number of photons in the pulse with the volume of the pulse being kept constant.

Let us take, as an example, a laser pulse characterized by $I = 2 \times 10^{13}$ W cm^{-2}, $r_f = 12\,\mu$m, and $T_p = 100$ psec. Substituting these values into Eq. (4.1.5) produces a pulse energy equal to 9.04 mJ. With $I = 7 \times 10^{13}$ W cm^{-2} and all other parameters kept the same, we obtain $E_p = 31.6$ mJ. These results are in excellent agreement with those found by Muller and Tip [29].

Consider next the laser pulse mentioned above as an aggregate of spherical cells, each having a volume

$$V_c = \frac{4}{3}\pi r_\gamma^3 \ , \tag{4.1.6}$$

where r_γ is the photon radius. This volume is the same as the photon volume. Substituting Eq. (4.1.3) into Eq. (4.1.6) yields a cell volume of

$$V_c = \eta^3 (8.21 \times 10^{-10}) \lambda^3 \ . \tag{4.1.7}$$

The number of cells C_0 in the pulse is then

$$C_0 = \frac{V_p}{V_c} \ . \tag{4.1.8}$$

Substituting V_p from Eq. (4.1.4) and V_c from Eq. (4.1.7) into Eq. (4.1.8), the number of cells becomes

$$C_0 = (1.15 \times 10^{18}) \eta^3 \frac{r_f^2 T_p}{\lambda^3} \ . \tag{4.1.9}$$

The number of photons N_0 in the pulse is

$$N_0 = \frac{E_p}{\hbar\omega} \ , \tag{4.1.10}$$

where E_p is the pulse energy in Joules, given in Eq. (4.1.5), and $\hbar\omega$ is the photon energy in Joules. The number of photons in the pulse is also given by the product FV_p, where V_p is the pulse volume and F is the flux given by

$$F = \left(\frac{1}{3 \times 10^4} \right) \frac{I}{\hbar\omega} \ , \tag{4.1.11}$$

where F is in photons / m^3, I in W cm $^{-2}$, and $\hbar\omega$ in Joules. The factor $1/(3 \times 10^4)$ of Eq. (4.1.11) is inserted because of the specific units used in the equation. Due to this factor the flux units be-

come photons/m³ and not the usual photons/m² . The number of photons N_0 in the pulse can now be expressed as

$$N_0 = \left(\frac{1}{3 \times 10^4} \right) \frac{V_p I}{\hbar\omega} = F V_p , \tag{4.1.12}$$

where V_p is in m³, I in W cm $^{-2}$, and $\hbar\omega$ in Joules. Eq. (4.1.12) can be rewritten as

$$N_0 = \left(\frac{1}{3 \times 10^4} \right) \frac{\pi r_f^2 T_p I c}{\hbar\omega} . \tag{4.1.13}$$

Eq. (4.1.13) is in excellent agreement with the photon number derived by Shore *et al.* [30].

Now, let us think of the laser pulse as being an energy packet of volume V_p occupied by N_0 photons. Let the volume V_p consist of a number of elementary cells, each having a volume V_c, such that V_c is small compared with V_p. The probability W_N that V_c contains N photons can be found [31] and is given by

$$W_N = \frac{N_0!}{N!(N_0 - N)!} \left(\frac{V_c}{V_p} \right)^N \left(1 - \frac{V_c}{V_p} \right)^{N_0 - N} . \tag{4.1.14}$$

The probability that any given photon is in V_c is just the ratio V_c/V_p, and the probability that N given photons are simultaneously present in it is $(V_c/V_p)^N$. Similarly, the probability that a photon is not in V_c is $(V_p - V_c)/V_p$ and the probability that $N_0 - N$ photons are not in V_c is given by $[(V_p - V_c)/V_p]^{N_0 - N}$. In Eq. (4.1.14) a factor has been included which gives the number of all possible ways of choosing N out of N_0 photons, since the photons are not distinquishable.

Let $V_c \ll V_p$ and suppose that the number N is much smaller compared with the total number N_0 of photons. We may use the approximation $N_0! \simeq (N_0 - N)!\, N_0^N$ and neglect N in the expression $N_0 - N$ appearing in Eq. (4.1.14). As a result, we have

$$W_N = \frac{1}{N!}\left(N_0 \frac{V_c}{V_p}\right)^N \left(1 - \frac{V_c}{V_p}\right)^{N_0} . \tag{4.1.15}$$

But $N_0 V_c / V_p$ is just the mean number $\bar{N}$ of photons in the volume V_c. Introducing this quantity into Eq. (4.1.15), we have

$$W_N = \frac{\bar{N}^N}{N!}\left(1 - \frac{\bar{N}}{N_0}\right)^{N_0} . \tag{4.1.16}$$

Finally, using the formula

$$\lim_{n\to\infty}\left(1 - \frac{x}{n}\right)^n = e^{-x},$$

we may replace $(1 - \bar{N}/N_0)^{N_0}$, with N_0 large, by $e^{-\bar{N}}$ and obtain the probability distribution in the form

$$W_N = \frac{\bar{N}^N e^{-\bar{N}}}{N!} . \tag{4.1.17}$$

Eq. (4.1.17) is the *Poisson* formula. It is easily seen that it satisfies the normalization condition

$$\sum_{N=0}^{\infty} W_N = 1 . \tag{4.1.18}$$

W_N in Eq. (4.1.17) is a probability distribution; it has two maximum peaks corresponding to N set equal to $\bar{N} - 1$ and $\bar{N}$, respectively. So, for $\bar{N} = 2$, the maximum peaks of W_N are the first two peaks W_1 and W_2 respectively, (an average of 1 or 2 photons per cell). To clearly see this, a few graphs are given of W_N versus N for $\bar{N} = 2$, 4, 5, and 7 in Fig. 4.1. As $\bar{N}$ increases, the highest peak is shifted towards the right while the peaks on the left of the highest peak become smaller and

smaller and eventually disappear. It should be noted that Loudon [32] arrives at exactly the same photon distribution in a laser beam for the constant intensity case.

Based on our discussion of ATI in the previous chapters, it has become obvious that peak suppression is a very important characteristic. As the intensity increases, during experiments, the electron energy spectra are changed by shifting the highest peak to the right while the peaks on the left are suppressed. Obviously there is a great similarity between what is observed in the ATI experiments and what Eq. (4.1.17) describes. An electron energy spectrum is at a one-to-one correspondence with the graph of W_N versus N, with N representing the number of photons absorbed while W_N is equivalent to the relative peak heights. We shall apply next our theory to above threshold ionization. Electron energy spectra will be predicted through our model and will be compared to energy spectra produced in experiments. Before we attempt to do this, however, we shall give the formulation of our ATI model.

4.2 THE ATI MODEL

In a typical ATI experiment, described in Chapter 2, a vacuum chamber is filled with a spectroscopically pure rare gas at a very low static pressure, so that no collision occurs among the ionized atoms. A laser pulse is focused into the chamber, and its intensity is adjusted to produce 1 to 10^4 electron-ion pairs in the interaction volume. The volume of the laser pulse is the same as the interaction volume. The pulse contains elementary cells the size of which is the same as the photon size. A typical cell contains a number N of photons which completely overlap; that is, they all crowd together forming a "bunch" the volume of which is the same as the volume of one photon. The resulting energy is N times larger. The size of a typical atom is of the order of the photon size and the probability of two atoms occupying the same cell is negligible since the number of atoms in the interaction volume is very small compared to the number of cells. Hence, an atom is affected by one cell only. In a laser beam, a typical cell will contain a mean number $\bar{N}$ photons, and an

atom located in that cell will absorb $\bar{N}$ photons. This energy will be transfered to only one electron, and if it is large enough, the electron will leave the interaction volume. Eq. (4.1.17) is now an equation where ionization probabilities can be calculated. For example, W_N is the probability that an electron absorbs N photons. Every beam is characterized by a mean number $\bar{N}$ of photons per cell as calculated in section 4.1. So, during an interaction of a laser beam with an atom, the highest ionization probability will correspond to an electron absorbing $\bar{N}$ or $\bar{N}-1$ photons. Thus, by applying Eq. (4.1.17), we can produce electron energy spectra which are actually graphs of W_N versus N for different values of $\bar{N}$. The energy of the electron coming out will be the difference of the energy of the number of photons absorbed and the ionization energy. For example, in the case of Xe the ionization energy E_i is about $11\hbar\omega$ Joules at a wavelength $\lambda = 1064$ nm. This means that an electron needs to obtain a minimum energy of E_i. If it obtains an energy of say $13\hbar\omega$ Joules during the interaction with the laser beam, then the electron will exit the beam with energy of $E_e = 2\hbar\omega$ Joules.

At this point, we see that with the help of our ATI model, along with the laser beam model we can actually calculate the volume of the pulse, given the duration of the pulse, as well as the number of photons in the pulse. Moreover, the cell volume can be found through the photon radius, and consequently the number of cells in the pulse can be calculated. Then, the mean number $\bar{N}$ can also be found by simply dividing the number of photons by the number of cells in the pulse. So, through our model, given the laser pulse duration, the radius of focus of the laser beam, the laser intensity and finally the laser wavelength, the energy of the electrons released can be calculated and electron energy spectra can be produced for different intensities or pulse durations. The next step then will be to compare these spectra to experimental spectra. This will be undertaken in the next section.

4.3 CALCULATIONS AND COMPARISONS WITH EXPERIMENTS

In this section, we shall limit the discussion to specific experiments on above threshold ionization for which electron energy spectra have been produced. Using our work in section 4.1 and the characteristics of the laser beam used in the experiments, we will produce the predicted electron energy spectra and quantitatively compare them with the spectra produced in the experiments.

We first start with an experiment on the 11-photon ionization of xenon at a laser wavelentgh of 1064 nm which was conducted by Kruit *et al.* in 1983 [3]. A commercial Nd-YAG laser was used, giving (10-15) ns pulses of up to 1 Joule per pulse at a rate of 10 Hz. For this experiment, only the central part of the beam was selected and focused with a lens of focal length 12 mm to a diameter of 8 μm. For 1064-nm radiation, the maximum pulse energy E_p was about 32 mJ, corresponding to an intensity of 7×10^{13} W cm^{-2} [29].

The results of the above experiment are shown in Fig. 4.2 which shows electron energy spectra from ionization of xenon by 1064-nm photons at pulse energies of 32 mJ and 22 mJ, and xenon pressures of 0.004 Pa and 0.16 Pa, respectively. The pressures are chosen in such way that the total electron signal in each spectrum is 25-50 electrons per pulse. The pulse duration is 10 psec.

The number of photons N_0 in the laser beam is the energy of the pulse E_p divided by the photon energy $\hbar\omega = 2\pi\hbar(c/\lambda)$, as seen in Eq. (4.1.10). The wavelength of 1064 nm yields a photon energy equal to 1.17 eV, or 1.87×10^{-19} Joules, and the pulse energy of 22 mJ yields a number of photons $N_0 = 1.75 \times 10^{17}$. In our model, the pulse energy E_p is directly proportional to the laser intensity I, and in this experiment $I = 4.8 \times 10^{13}$ W cm^{-2}.

Eq. (4.1.12) gives the number of photons N_0 in terms of the pulse volume V_p, the intensity I, and the photon energy $\hbar\omega$. From this equation we solve for the pulse volume and we find $V_p = 1.37 \times 10^{-11}$ m^3. As we discussed above, in the ATI model, the laser pulse contains cells each having a volume V_c given in Eq. (4.1.7), and which is proportional to the third power of the wavelength λ. Now, substituting Eq. (4.1.7) into Eq. (4.1.8) the number of cells C_0 equals

$\eta^{-3}(1.387 \times 10^{16})$, where η is a free dimensionless parameter of O(1). The mean number of photons per cell $\bar{N}$ equals N_0 divided by C_0; in this case, $\bar{N} = 8.475\eta^3$.

The parameter η is adjusted so that the mean number of photons per cell $\bar{N}$ equals to 11, or $8.475\eta^3 = 11$. This yields the value $\eta = 1.09$. The justification for doing this lies in the fact that a xenon electron needs to absorb at least 11 1064-nm photons in order to be able to exit the interaction volume and be detected. Now, using Eq. (4.1.17), the ionization probabilities corresponding to $\bar{N} = 11$ can be calculated for different values of N starting at $N = 11$. A comparison of experimental and theoretical results corresponding to these values is shown in Fig. 4.3.

We will concentrate next on the upper spectrum in Fig. 4.2, where the pulse energy E_p is 32 mJ. The first two peaks are the maximum peaks of the spectrum, and they correspond to an electron absorbing 11 and 12 photons, respectively. The energy value given above corresponds to a number of photons $N_0 = 1.709 \times 10^{17}$, and an intensity $I = 7 \times 10^{13}$ W cm^{-2}. The pulse volume V_p is calculated from Eq. (4.1.12) and we get $V_p = 1.37 \times 10^{-11}$ m^3; it is the same as in the first case. The number of cells is $C_0 = \eta^{-3}(1.387 \times 10^{16})$, again the same as in the first case. The mean number of photons per cell $\bar{N}$ equals N_0/C_0 and we have $\bar{N} = 12.327\eta^3$. The parameter η is now adjusted so that the mean number of photons per cell is $\bar{N} = 12$; this yields $\eta = .99$. The ionization probabilities in Eq. (4.1.17) are calculated for different values of N starting at $N = 11$, and the comparison between the experimental and theoretical results corresponding to these values is shown in Fig. 4.4.

A third comparison relates to the experiment on ionization of xenon performed by Lompre' *et al.* in 1985 [4]. The experimental conditions in this case are identical to the ones described in the beginning of section 4.2. The laser wavelength is $\lambda = 1064$ nm. The laser pulse duration is $T_p = 50$ psec, and the intensity is $I = 3.6 \times 10^{13}$ W cm^{-2}. The envelope of the peaks of the electron enegry spectrum at three different values of the laser intensity is shown on Fig. 4.5. Spectrum (c) is of our interest due to the large number of data as compared to spectra (a) and (b). The radius of the focus here is not stated. For this reason we assume it is $r_f = 15\ \mu$m, which is a typical radius of focus for such lasers. Having the values just specified we are able to calculate the pulse energy, the total number of photons, the pulse volume, the number of cells, and finally the mean number of photons per cell. Proceeding as in the previous cases, we obtain the values $E_p = 12.7$ mJ,

$N_0 = 6.784 \times 10^{16}$ photons, $V_p = 1.06 \times 10^{-11}$ m^3, $C_0 = \eta^{-3}(1.07 \times 10^{16})$ cells, and $\bar{N} = 6.34\eta^3$ photons per cell. Fig. 4.6 shows a comparison of the theoretical spectrum with spectrum (c) of Fig. 4.5. In this comparison the heights are scaled to match at $N = 16$, which yields $\eta = 1.36$.

In all three experiments discussed above, the rare gas utilized was xenon, which is the most frequently used gas in the majority of ATI experiments. In the comparisons with our theoretical model, the parameter η was adjusted so that the maximum peaks of the theoretical and experimental peaks matched. In the first comparison, the mean number of photons was given as $\bar{N} = 8.475\eta^3$, and η was adjusted so that $\bar{N} = 11$ photons/cell, yielding $\eta = 1.09$; in the second comparison, we found $\eta = .99$, corresponding to $\bar{N} = 12$ photons/cell; finally, in the third comparison, we found $\bar{N} = 16$ photons/cell after setting $\eta = 1.36$.

The comparison of the theoretically predicted spectra and the ones produced in the experiments shows an overall good agreement for the first two cases. Differences occur, however, between the peaks located close to the maximum peaks. The slope of the envelope of the theoretical peaks is greater than the slope of the envelope of the experimental peaks; that is, the predicted peaks do not decrease (on the right of the maximum peaks) as fast as the experimental ones. It should be noted, however, that the slopes become equal at the right edge of the spectra. In the third case the results are quite different. The first experimental peak, corresponding to $N = 11$, is absent. There is good agreement for the next seven peaks. In the range $N = 19$ to $N = 23$ there is a relatively big difference between peaks, whereas the peaks corresponding to $N = 24$ are close to each other in magnitude.

There is a distinct difference between the first two cases and the third one. In the former the main differences between theoretical and experimental results appear in the neighborhood of the maximum peaks, while the right half of the spectra exhibit good agreement. The opposite happens in the third case, where the peaks in the neighborhood of the maximum are of about the same magnitude, while the rest are different except for the last set.

Referring to the first two comparisons shown in Figs 4.3 and 4.4, it should be noted that a better agreement would have resulted if we had set the theoretical spectra so that their maximum peaks occurred at a number N less than 11 or 12. The envelope of the peaks to the right of the

maximum then would have been smaller and thus closer to the experimental slope. Our model, however, is consistent with the ionization condition, according to which a xenon electron will be detected if it absorbs a minimum of 11 photons at a wavelength of 1064 nm. Concerning now the third case, an examination of Fig. 4.5 indicates that there is an inconsistency among envelopes (a), (b), and (c). As seen, envelopes (a) and (b) correspond to an intensity of $0.9I_s$ and $1.1I_s$, respectively, while the intensity for envelope (c) is $3I_s$; this means that the area under curve (c) must be about 3 times the area under curve (b). Obviously this cannot be the case. Another way of interpreting envelope (c) compared to envelopes (a) and (b) is that for that intensity much more ionization events occured resulting in a stronger signal. This, however, can cause space charge effects; the latter may be the reason for the absence of the first peak in the experimental envelope. As we mentioned earlier, space charge effects can be avoided provided there are as few as possible ionization events occurring in the interaction volume. Space charge effects cause the suppression, or even the disappearance, of the slow electron peaks. In Ref. [20], it is mentioned that the disappearance of only the first peak could be attributed to space charge effects, laser pulse duration effects, and angular distributions occurring to varying degrees in some of the experiments.

Through our model, we can predict ATI spectra for a given ionization experiment provided information on the laser beam is given for every intensity value. This information includes the laser intensity, the radius of focus r_f of the beam, the pulse duration, and the laser wavelength. A crucial quantity is the radius of focus r_f which changes as the intensity changes; unfortunately it is not specified in numerous experiments. We suggest to people conducting ATI experiments to provide the complete information on the laser beam since its characteristics change for different intensity values.

According to our model, a laser pulse contains a large number (the order of 10^{16}) of elementary cells occupied by photons. One may wonder how many photons can be "located" in a typical cell. Obviously there must be a limit on the number of photons N_0 occuping a small volume i.e., the pulse volume. The number of photons per cell N depends on the cell size, so that more photons of the same wavelength can be "packed" in larger cells. As the intensity increases, the number of photons N_0 in the pulse increases. When N_0 is too large for that particular pulse, the volume V_p

is expected to expand. Now, if one tries to keep V_p constant, then N_0, initialy increasing linearly with V_p, will start to increase in a slower fashion until it reaches a *saturation*, after which no more photons can be packed in the pulse volume and $N_0 = N_{max}$. We assume here that N_0 increases as $1 - \exp(-x)$ and write the equation

$$N_0 = N_{max}[1 - \exp(-I/I_s)], \tag{4.3.1}$$

where I_s is the saturation intensity given in experiments, and I is the intensity of the laser pulse. In this case, the shift of the maximum peak of the spectrum will not be proportional to the increase in intensity. This characteristic is observed in numerous experiments [4,6,12]. However, it is not mentioned whether the pulse volume varies for different intensity value.

4.4 CONCLUSION

In this chapter we have provided a simple theoretical model for above threshold ionization. The laser beam is represented as a *cylinder* consisting of elementary cells, which are *spheres* of volume equal to the photon volume. There are N photons in a cell which completely overlap; that is, they all crowd together forming a "bunch", the volume of which is the same as the photon volume. The energy, however, is the sum of the energies of the individual photons. There are very few atoms located inside the interaction volume so that the possibility of a cell being occupied by two or more atoms is negligible. The atom obtains all the cell energy and transfers this energy to one electron only. If the amount of this energy is equal or greater to the ionization energy the electron will come out of the interaction volume (the laser beam). This results in the formation of A^+ ions, where A is a rare gas atom, i.e., Xe, Ne, etc.

As we emphasized before, our ATI model is a simple model not taking into account some physical effects which may be important. For example, one might ask why there should only be A^+ ions formed in the interaction volume. It is in fact possible to have multi-electron excitation,

where an atom loses 2 or more of its electrons during above threshold ionization [9,10,11]. In this case our model should be modified by taking into account the fact that the atom transfers its energy to more than one of its electrons. In most of the ATI experiments [3,4,6] the number A^{++} ions created in the interaction volume is very small and almost never considered when studying ATI.

Our model assumes that nothing happens to the electron *during* its exit from the beam. If space charge effects are a factor in ATI, then the slower moving electrons will not be able to exit the beam due to the net positive charge left behind by the fast moving electrons (the electrons with high kinetic energies). The effect of this will be the distortion of the actual electron energy spectrum due to a decrease of the peaks on the left of the spectrum, or even a complete elimination of the first electron peak of the energy spectrum.

The intensity is assumed constant throughout the pulse. This is not a very realistic situation. The detailed structure of the laser pulse has to be taken into account before a meaningful comparison with experimental data can be attempted [18]. As mentioned before, the laser beams used in ATI experiments are characterized by extremely high intensities obtained in tightly focused picosecond pulses, as well as in the spikes of multimode nanosecond laser pulses. A complete knowledge of the instantaneous intensity is crucial when studying ATI. However, it is almost impossible to measure the instantaneous intensity when obtained from the spikes of multimode nanosecond pulses. As for the tightly focused picosecond pulses the intensity quoted is not usually trusted to better than a factor of 2 [21].

In Chapter 3, the theory that produced the photon model is built primarily on the free particle state of the photon and no full interaction theory has been introduced. As a result, our ATI model does not account for photon-photon interaction. Developing a full interaction theory will help us account for multiphoton interactions, as well as the effects of such interactions on the physical system. Such an interaction theory may dramatically change our ATI model.

Effects of angular distribution of electrons are not considered in our model. Taking into account angular distributions does not change the intensity dependence of electron peaks, but does change the relative amplitude of electron peaks. This effect could contribute to the disappearance of the first electron peak relative to the subsequent peaks on a spectrum [20].

Different polarizations of the laser beam are not considered in our ATI model. It has been shown however, experimentally [6,21] that peak suppression is more prominent for circular polarization than for linear polarization. There is no distinction in our model between linear and circular polarization.

In spite of all these drawbacks, our model exhibits relatively good agreement with experimental data. Despite its simplicity, it can qualitatively, as well as quantitatively, explain peak suppression, which is one of the most important characteristics in ATI. As discussed in the previous chapters, all the ATI theories must be modified when dealing with high intensity values and new approximations should be made in order to predict the energy distribution of the freed electrons. A great advantage of our theory over the others is that it applies for any intensity value and no such approximations are needed. Present data on ATI are limited to the highest intensity values available today. This restricts a full comparison of our model because, even though it can produce electron energy spectra at very high intensity values, there are no corresponding experiments.

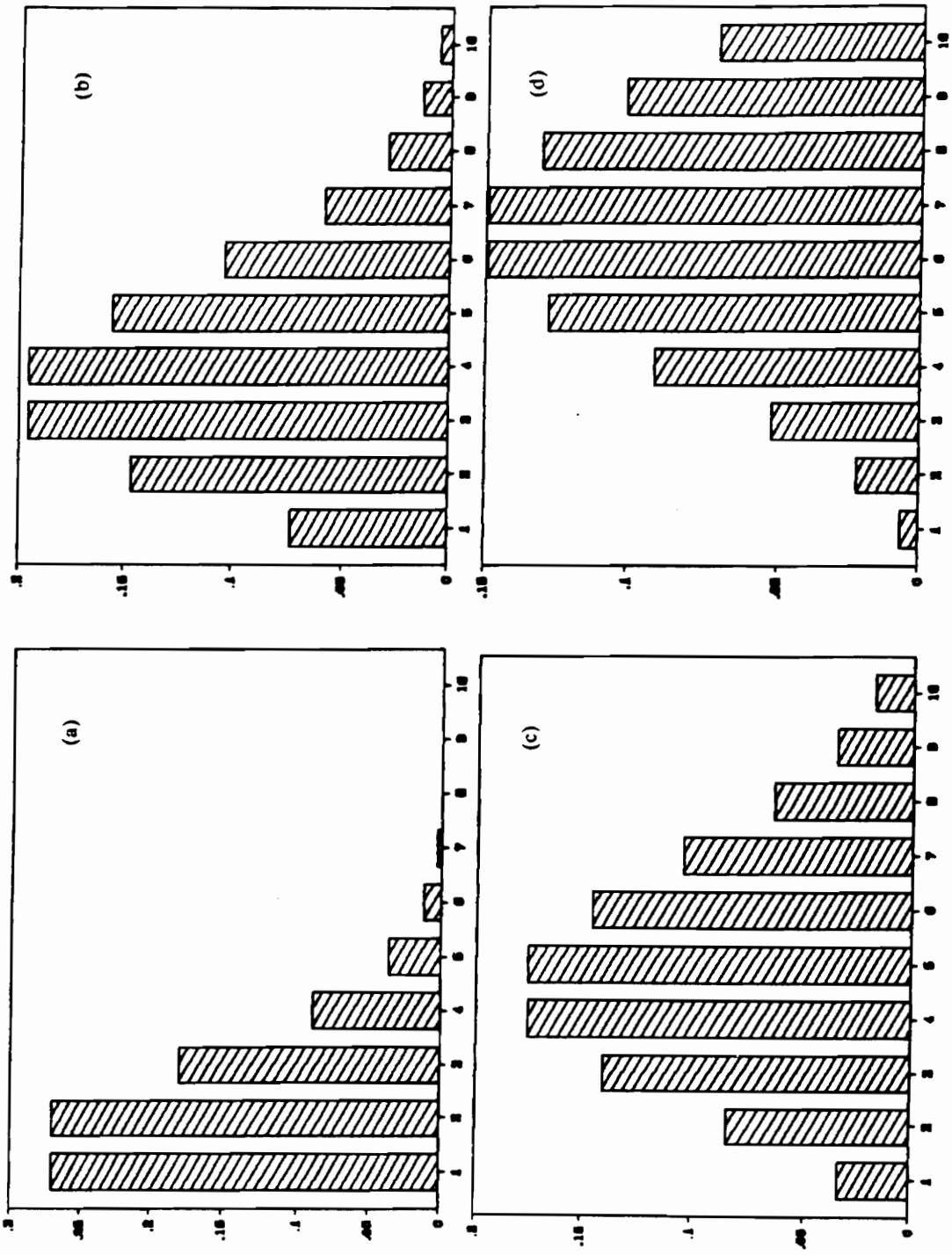

Fig. 4.1. Poisson Formula: W_N versus N for different $\overline{N}$, (a) $\overline{N} = 2$, (b) $\overline{N} = 4$, (c) $\overline{N} = 5$, and (d) $\overline{N} = 7$.

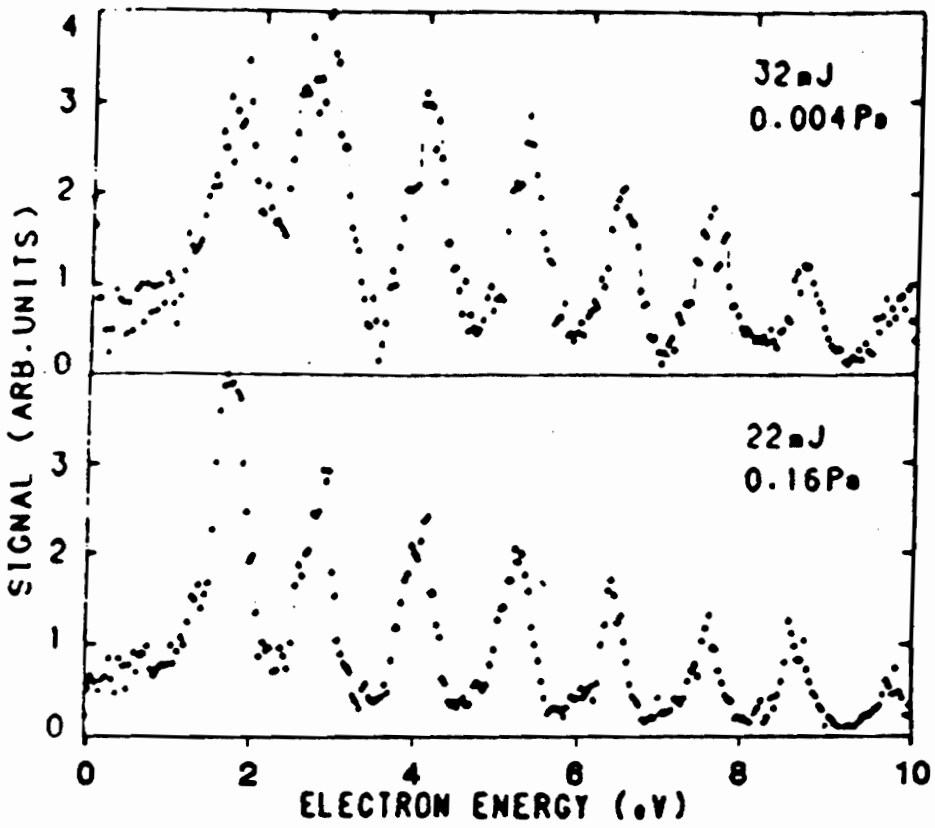

Fig. 4.2. Electron spectra from multiphoton ionization of xenon at 1064-nm. The vertical scales are normalized. The pulse energy E, and pressure at which each spectrum is taken is given in the figure [29].

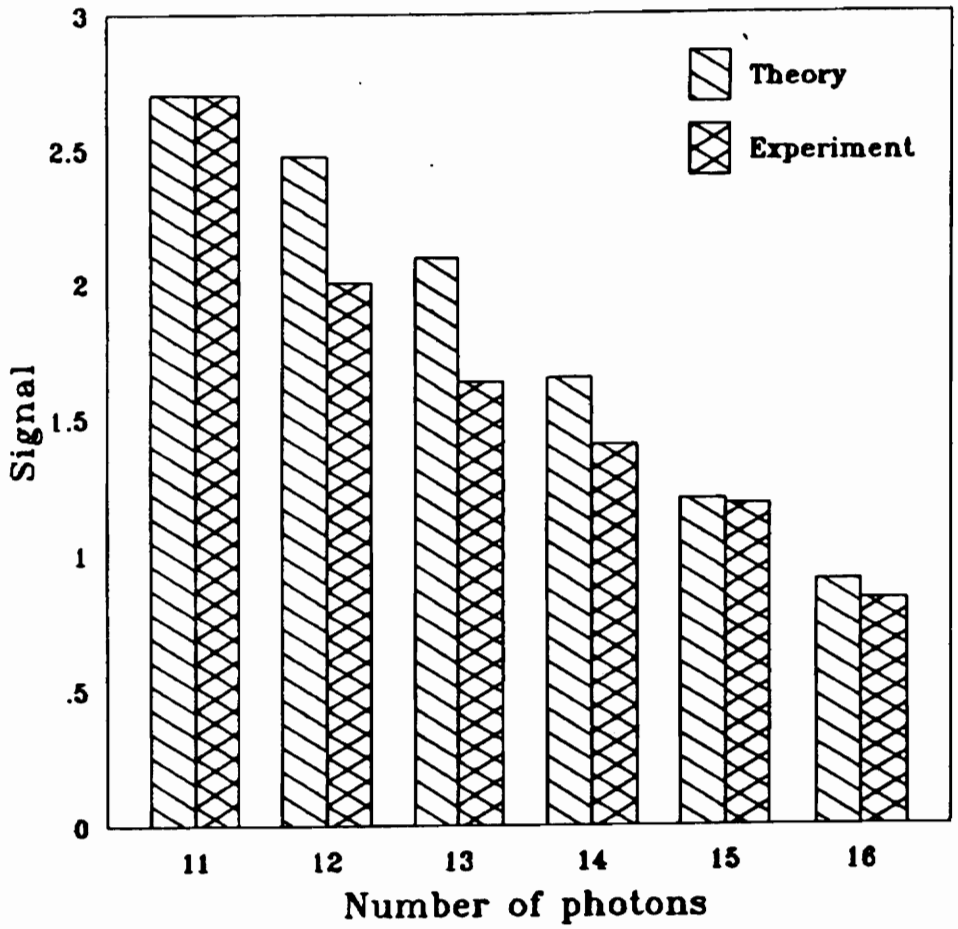

Fig. 4.3. Comparison corresponding to the lower electron energy spectrum of Fig. 4.2 and Poisson formula with $\bar{N} = 11$.

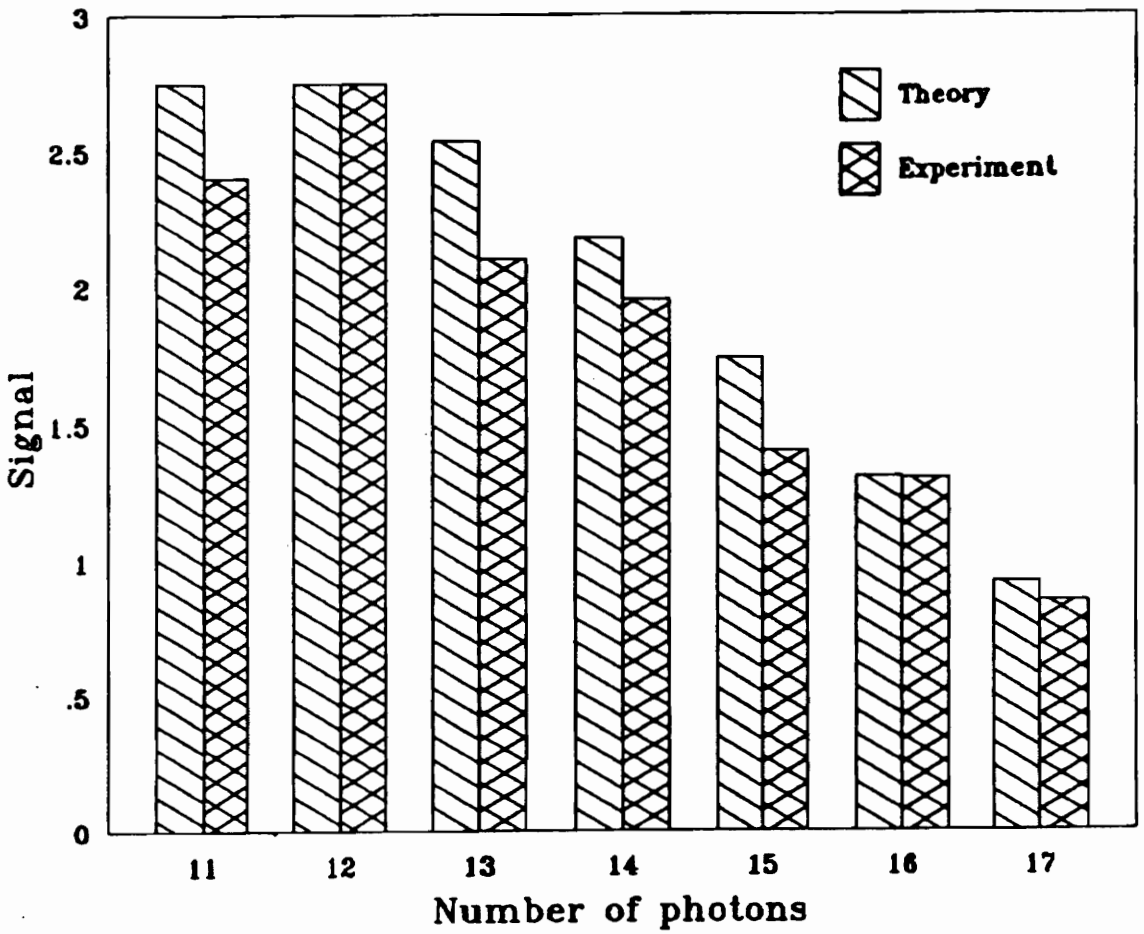

Fig. 4.4. Comparison corresponding to the upper electron energy spectrum of Fig. 4.2 and Poisson formula with $\bar{N} = 12$.

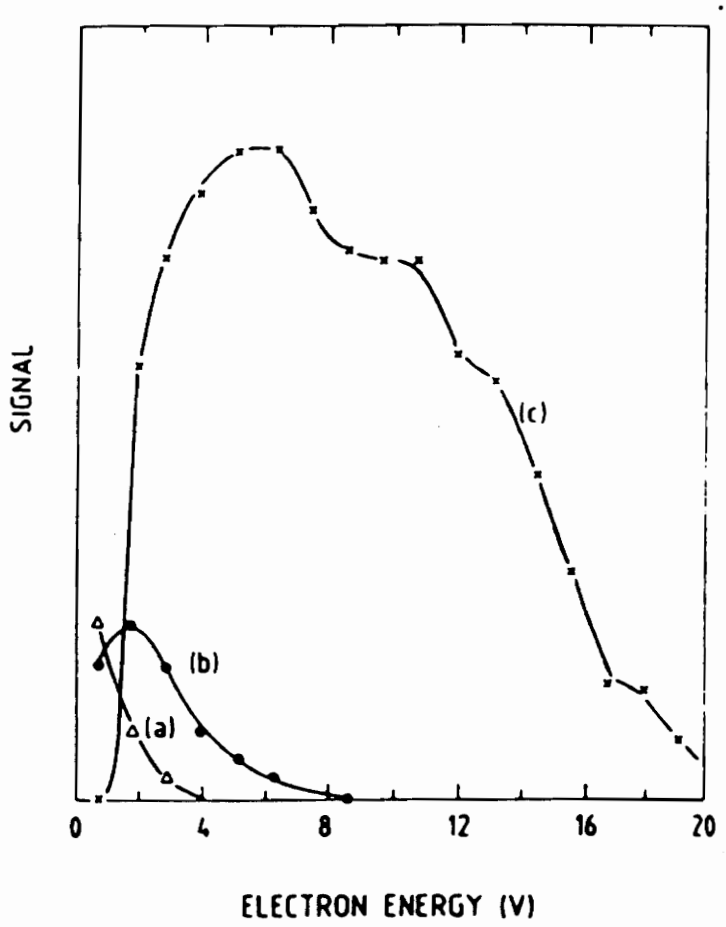

Fig. 4.5. Multiphoton ionization of xenon at 1064 nm. The envelope of the peaks of the electron energy spectrum at three different values of the laser intensity: (a) $0.9I_s$, (b) $1.1I_s$, and (c) $3I_s$, with $I_s = 1.2 \times 10^{13}$ W cm^{-2} [4].

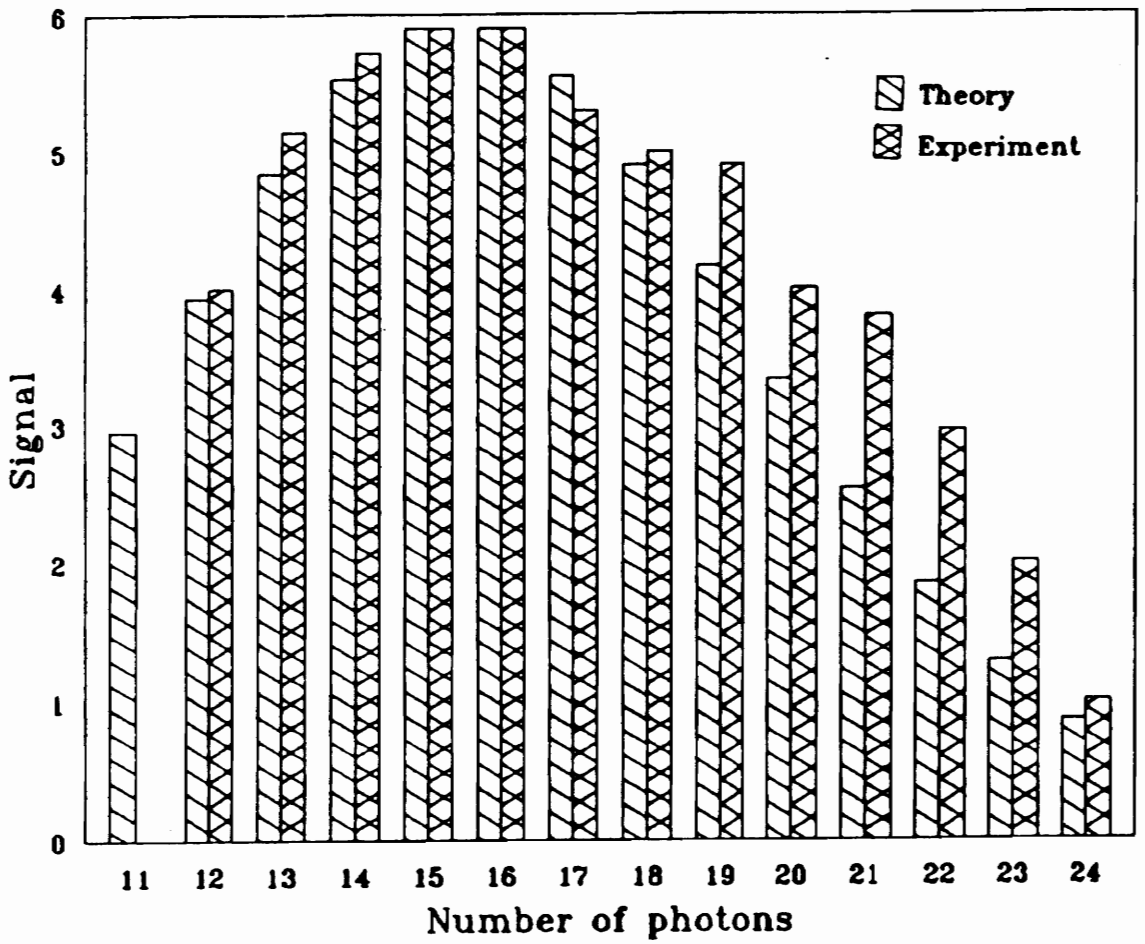

Fig. 4.6. Comparison corresponding to spectrum (c) of Fig. 4.5 and Poisson formula with $\overline{N} = 16$.

REFERENCES

1. G. S. Voronov and N. B. Delone, 'Ionization of the xenon atom by the electric field of ruby laser', JEPT Lett. **1,** 66 (1965).

2. P. Agostini, F. Fabre, G. Mainfray, G. Petite and K. N. Rahman, 'Free-free transition following six-photon ionization of xenon atoms', Phys. Rev. Lett. **42,** 1127 (1979).

3. P. Kruit, J. Kimman, G. H. Muller and J. M. van der Wiel, 'Electron spectra from multiphoton ionization of xenon at 1064, 532 and 355 nm', Phys. Rev. A **28,** 248 (1983).

4. L. A. Lompre', A. L'Huillier, G. Mainfray and C. Manus, 'Laser-intensity effects in the energy distributions of electrons produced in multiphoton ionization of rare gases', J. Opt. Soc. Am. B **2,** 1906 (1985).

5. T. S. Luk, T. Graber, H. Jara, U. Johan, K. Boyer and K. C. Rhodes, 'Subpicosecond ultraviolet multiphoton electron spectroscopy of rare gases', J. Opt. Soc. Am. B **4,** 847 (1987).

6. P. H. Bucksbaum, M. Bashkansky, R. R. Freeman, T. J. McIlrath and L. F. DiMauro, 'Suppression of multiphoton ionization with circularly polarized coherent light', Phys. Rev. Lett. **56,** 2590 (1986).

7. L. V. Keldysh, 'Behavior of non-metallic crystals in strong electric fields', JETP **6,** Soviet Phys. 763 (1958).

8. L. Pan, 'The Volkov-like continuum', J. Modern Optics **36,** 877 (1989).

9. F. Yergeau, S. L. Chin and P. Lavinge, 'Multiple ionisation of rare-gas atoms by an intense CO_2 laser (10^{14} W cm^{-2})', J. Phys. B **20,** 723 (1987).

10. P. Lambropoulos and X. Tang, 'Multiple excitation and ionization of atoms by strong lasers', J. Opt. Soc. Am. B **4,** 821 (1987).

11. N. B. Delone, I. P. Zapesochnyi, B. A. Zon and V. V. Suran, ' Two- electron multiphoton ionization of atoms', Izvestiya Akademii Nauk SSSR, Seriya Fizicheskaya, **45,** 1085 (1981).

12. F. Trombetta, S. Basile and G. Ferrante, 'Multiphoton one-step ionization of helium at 1064 nm', J. Modern Optics **36,** 891 (1989).

13. R. H. Reiss, 'Effect of an intense electromagnetic field on a weakly bound system', Phys. Rev. A **22,** 1786 (1980).

14. R. H. Reiss, 'Spectrum of atomic electrons ionised by an intense field', J. Phys. B **20,** L79 (1987).

15. A. Messiah, *Quantum mechanics* , Vol. 1 (North-Holland, Amsterdam, 1961).

16. P. Agostini and G. Petite, 'Photoelectric effect under strong irradiation', Contemp. Phys. **29,** 57 (1988).

17. J. Kupersztych, 'Inverse half-bremsstrahlung in multiphoton ionisation of atoms in intense light beams', Europhys. Lett. **4,** 23 (1987).

18. W. Becker, R. R. Schlicher, M. O. Scully and K. Wodkiewicz, 'Role of final-state effects in Above-Threshold Ionization', J. Opt. Soc. Am. B **4,** 743 (1987).

19. F. Yergeau, G. Petite and P. Agostini, 'Above-threshold ionisation without space charge', J. Phys. B **19,** L663 (1986).

20. L. A. Lompre', G. Mainfray, C. Manus and J. Kupersztych, 'The energy distributions of electrons produced in multiphoton ionisation of rare gases', J. Phys. B **20,** 1009 (1987).

21. G. Petite, P. Agostini and F. Yergeau, 'Intensity, pulse width and polarization dependence of above-threshold-ionization electron spectra', J. Opt. Soc. Am. B **4,** 765 (1987).

22. A. M. Shaarawi, I.M. Besieris and R. W. Ziolkowski, 'A nondispersive wave packet representation of photons and the wave-particle duality of light', submitted to Found. Phys.

23. J. N. Brittingham, 'Focus wave modes in homogeneous maxwell's equations: transverse electric mode,' J. Appl. Phys. **54,** 1179 (1983).

24. R. W. Ziolkowski, 'Exact solutions of the wave equation with complex source locations,' J. Math. Phys. **26,** 861 (1985).

25. I. M. Besieris and A. M. Shaarawi, 'A linear superposition theory based on constrained bilinear invariants of a factorized embedded operator,' presented at the Joint IEEE AP-S / URSI Symposium, Blacksburg, VA June (1987).

26. I.M. Besieris, A. M. Shaarawi and R. W. Ziolkowski, J. Math. Phys. **30,** 1254 (1989).

27. A. M. Shaarawi, I.M. Besieris and R. W. Ziolkowski, submitted to Phys. Rev. A.

28. J. E. Huheey, *Inorganic chemistry principles of structure and reactivity* , 2nd Edition, (Harper and Row publishers, 1978).

29. G. H. Muller and A. Tip, 'Multiphoton ionization in strong fields', Phys. Rev. A **30,** 3039 (1984).

30. B. W. Shore and K. C. Kulander, 'Generation of optical harmonics by intense pulses of laser radiation', J. Modern Optics **36** 857 (1989).

31. L. D. Landau and E. M. Lifshitz, *Statistical Physics* , 3rd Edition Part 1, Translated by: J. B. Sykes and M. J. Kearsley, (Pergamon Press, Oxford, 1978).

32. R. Loudon, *The quantum theory of light* (Clarendon, Oxford, 1983).

VITA

Argyrios Chatzipetros was born in Nea Selefkia, Northwestern Greece, December 7, 1964. He graduated in 1982 from Igoumenitsa High school in Greece, with honors and received the Greek Mathematics Society award after participating in a national competition.

After he came to the United States, he attended Central New England College in Worcester Massachusetts where he received his Associate's in Electronic Engineering. There he also received the Outstanding Engineering Student Award.

In 1984 he transfered to Virginia Polytechnic Institute and State University to continue his undergraduate studies and graduated in March 1987 receiving his B.S. degree in Electrical Engineering.

In the Fall of 1987 Mr. Chatzipetros returned to Virginia Polytechnic Institute and State University to pursue graduate studies. During his graduate studies he has been engaged in research involving ionization of atoms by intense lasers, propagation of directed electromagnetic energy, and phase-space beam methods.